



Thermite-for-demise (T4D): experiments and numerical modelling on solar array drive mechanism mock-ups containing thermite in an arc-heated wind tunnel

Alessandro Finazzi¹ · Dennis Daub² · Filippo Maggi¹ · Christian Paravan¹ · Stefano Dossi³ · Tobias Lips⁴ · Geert Smet⁵ · Kobyé Bodjona⁵

Received: 9 September 2024 / Revised: 16 December 2024 / Accepted: 2 February 2025

© The Author(s) 2025

Abstract

The ESA-TRP SPADEXO project investigated the use of thermites to provide additional enthalpy to a spacecraft re-entering towards the Earth, with the objective of limiting its casualty risk on ground. Steel mock-ups inspired by the geometry of solar array drive mechanisms were filled with thermite and placed in DLR's L2K arc-heated hypersonic wind tunnel. In each of these samples, a set of thermocouples was installed to monitor ignition and propagation of the heat generated by the reaction. One of the thermocouples was placed in a hole machined inside the mock-up wall to monitor temperature evolution in proximity of the pyrotechnic charge, without the risk of losing the sensor due to the ignition of the thermite. The main objective of these tests was to study the dependence of the heat transferred from the internal charge to the surrounding structure from the filling level. Results showed that higher thermite filling resulted in higher transferred enthalpy. In the presence of a large thermite amount, the reaction led to the formation of a dense liquid drop close to the side wall, causing significant heat transfer towards the wall of the mock-up. Tests were rebuilt using the SCARAB re-entry software, extended with a dedicated model to represent the ignition of an internal charge. Ignition and heat transfer were adequately described by the model in most of the test configurations. Specific parameter tuning was needed for the highest filling factor tested in this work, highlighting the influence of reaction products internal dynamics on the heat transfer processes.

Keywords Thermite · Design for demise · Aluminum · Iron oxide · Arc-heated wind tunnel

✉ Filippo Maggi
filippo.maggi@polimi.it

Alessandro Finazzi
alessandro.finazzi@polimi.it

Dennis Daub
dennis.daub@dlr.de

Christian Paravan
christian.paravan@polimi.it

Stefano Dossi
stefano.dossi@reactivepowders.com

Tobias Lips
t.lips@htg-gmbh.com

Geert Smet
Geert.Smet@esa.int

Kobyé Bodjona
Kobyé.Bodjona@esa.int

¹ Department of Aerospace Science and Technology, Politecnico di Milano, via La Masa, 34, 20156 Milan, Italy

² Supersonic and Hypersonic Technologies Department, Institute of Aerodynamics and Flow Technology, Deutsches Zentrum für Luft- und Raumfahrt e.V. (DLR), Linder Höhe, 51147 Köln, Germany

³ ReActive Powder Technology s.r.l., via Lambro, 7/3, 20068 Peschiera Borromeo, Italy

⁴ HTG-Hyperschall Technologie Göttingen GmbH, Am Handweisergraben, 13, 37120 Bovenden, Germany

⁵ ESTEC, European Space Agency, Keplerlaan, 1, 2200 AG Noordwijk, The Netherlands

1 Introduction

The need for removing man-made objects from Low Earth Orbit (LEO) is becoming more and more stringent every year. The evolution of the in-orbit population is monitored each year by the European Space Agency (ESA) in its *Annual Space Environment Report* [1]. In the last decade, the reduction of launch cost [2], the tendency toward miniaturization, and the growing displacement of megaconstellations led to a steep increase in the number of spacecraft delivered to orbit. Even if the benefits coming from the rising exploitation of space are unquestionable, the associated risks should also be considered. The higher the number of objects in a certain region, the higher the risk of collisions, possibly leading to catastrophic scenarios such as the one described by Kessler in 1978 [3]. It has been estimated that one-third to one-half of the LEO capacity to sustain long-term space activity has already been saturated [4].

The responsible disposal of space objects at the End of their Operative Life (EOL) is the only possible solution to limit the impacts of space activities. The Inter-Agency Space Debris Coordination Committee (IADC) was established to coordinate the efforts of the main space agencies toward a more sustainable future. One of the main results of its activities was the definition of a set of guidelines to be adopted internationally [5]. For the LEO region, one of the main prescriptions is the removal of the spacecraft from orbit after EOL, in the form of an atmospheric re-entry. The disposal should be performed no later than 25 years after the end of operations and with a reliability of at least 90%. Some entities implemented even stricter requirements: for example, ESA and the Federal Communications Commission (FCC) restricted the maximum residence time in LEO after the end of operations to 5 years [6, 7]. In this context, a significant increase of spacecraft re-entries in the next years is inevitable.

The aerothermal heat load experienced by a re-entering spacecraft could not be sufficient to completely ablate all space objects upon re-entry. Some fragments could reach the ground, leading to non-negligible casualty risk. Technical solutions can help limit this hazard. The first strategy is to perform a final high-thrust maneuver to make the derelict spacecraft impact on an uninhabited area. For more massive satellites, this procedure is typically prescribed by the space agencies, as the risks for people on ground are considered unacceptable. However, the lower risk on ground comes at a cost. In most cases, both a dedicated propulsion system and a propellant mass budget allocation are needed, possibly increasing the complexity of the system and the mission costs. Moreover, the final manoeuvre could fail, resulting in the uncontrolled re-entry of an even

more massive spacecraft. The other possible option is to aim for an uncontrolled re-entry from the beginning, if the casualty risk on the ground is deemed acceptable (generally, less than 10^{-4} [5]). Some design solutions could be adopted to make the space system as prone as possible to completely demise during re-entry, lowering in this way the expected casualty risk. This approach, named Design-for-Demise (D4D), can also be used to lower the expected casualty risk of an existing spacecraft design, aiming at reaching a level within the acceptability threshold. Moreover, D4D can be implemented as well on massive space objects to limit the aftermath in case of a failed re-entry maneuver. For these reasons, D4D became the preferred solution to limit the risks connected to the re-entry of ESA spacecraft [6]. Numerous D4D strategies have been investigated in recent years in the framework of the ESA Clean Space initiative [8]. Among them, some have the objective of aiding spacecraft demise by increasing the available enthalpy during the re-entry process. In particular, the exothermic reaction of some material placed on board could fulfill this task. Thermites, which are mixtures of metals and metal oxides, are good candidates for this role. Their high energetic density and their capability to react in vacuum are particularly attractive for space applications. They are relatively insensitive to external stimuli with respect to other energetic materials and, in this sense, intrinsically safer. Moreover, many different tuning leverages can be used to control the characteristics of their reactions, leading to a wide range of industrial applications (e.g., [9–11]). In this paper, the use of thermites to aid spacecraft demise will be referred to as Thermite-for-Demise (T4D).

To date, T4D has been investigated to a limited extent. The concept was formalized for the first time in a patent by the Centre National d'Études Spatiales (CNES) in 2011 [12], later followed by another patent filed by ESA in 2018 [13]. So far, three experimental campaigns have been carried out in hypersonic wind tunnels to verify this D4D strategy. The first, conducted by Monogarov et al. [14, 15], aimed to perforate a titanium plate, representative of a tank wall. The thermite, in pellet form, was encapsulated and attached externally to the target. The perforation of the plate was verified and the combustion of the charge was described numerically. A second test campaign was conducted in the framework of the ESA Exothermic Reaction-Aided Spacecraft Demise (ERASD) project [16]. In this case, the thermite was inserted into the structural voids of a ball-bearing unit (BBU) mock-up. The passive ignition of the charge was achieved by exploiting the aerothermal heat load, but the mock-ups were too massive and detailed to allow a precise quantification of the thermite effects on the demising component. The follow-up of this experimental campaign was part of the ESA-TRP "Spacecraft demise during re-entry

expedited using various exothermic reactions” (SPADEXO) project [17]. The initial results of these tests, on a simplified version of the BBU mock-ups used in the ERASD campaign, have already been presented in Ref. [18]. The primary objectives were to verify the feasibility of inducing partial demise of the sample using an internal thermite charge, to determine how the ignition temperature of the thermite charge could be adjusted through the inclusion of an activated fraction, and to assess the effects of varying ignition temperatures on the thermite reaction’s impact on the sample. These tests successfully demonstrated partial demise induced by the ignition of the embedded thermite charge. In addition, the passive ignition of the powder was effectively controlled through mechanical activation. Moreover, ESA’s Spacecraft Atmospheric Re-entry and Aerothermal Breakup (SCARAB) software was modified and used to predict the ignition of the pyrotechnic charge and its effects on the target vessel. In this paper, the results obtained for another geometry, inspired by a solar array drive mechanism (SADM), will be presented. The main objective of the tests on this geometry was to evaluate how the temperature increase in the surrounding structure during the thermite reaction depends on the filling level.

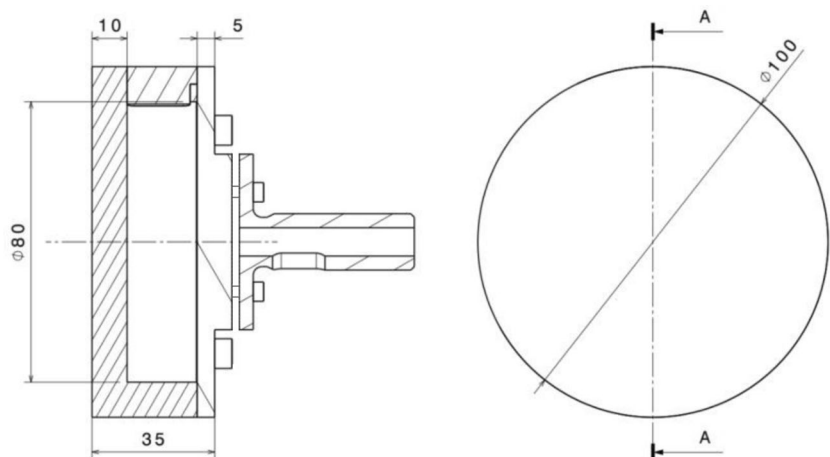
In Sect. 2, the mock-ups and the thermite charge will be detailed. The experimental facility and the numerical model used to rebuild the campaign will also be described. The results obtained will be reported and discussed in Sect. 3. Lastly, in Sect. 4 the main conclusions of this work will be outlined, together with a brief perspective on the future development of this technology.

2 Materials and methods

2.1 SADM mock-ups

The mock-ups used during the tests were designed to be as simple as possible and with an internal cavity able to host enough thermite to grant a measurable temperature increase. The geometry, inspired by the typical aspect ratio of SADM, resulted in the dimensions shown in Fig. 1. The external diameter of the samples was 100 mm and the height was 35 mm. The front face was 10 mm thick, while the thickness of all other walls was 5 mm. For safety reasons, the top of the mock-up was closed with a safety lid equipped with venting holes and held in place by a tantalum wire. This design was meant to limit the potential pressure build-up inside the geometry. The samples, made of 316 L steel, were mounted on a steel sample holder. Even if the arm sustaining the sample holder was water-cooled, the holder itself was not. To minimize heat conduction, steel screws were used to prevent direct contact between the sample and the holder. Six type K class 1 thermocouples were used to monitor the temperature evolution of the mock-ups during the tests. Their position and the labels used to refer to them are presented in Fig. 2. All thermocouples are centered with respect to the sample geometry, except for the one embedded in the thermite charge, which is placed at a distance of 10 mm from the bottom wall. This thermocouple was not present in the reference test, without the thermite charge. Another thermocouple was inserted into a hole drilled halfway through the thickness of the bottom wall. This design compensates for the potential failure of the other thermocouples, which are positioned within the cavity housing the thermite charge: sensors may fail at ignition, and for this reason they should no longer be considered reliable after this event. In contrast, the thermocouple embedded in the bottom wall is expected to remain functional and to provide reliable data throughout

Fig. 1 SADM mock-ups geometry



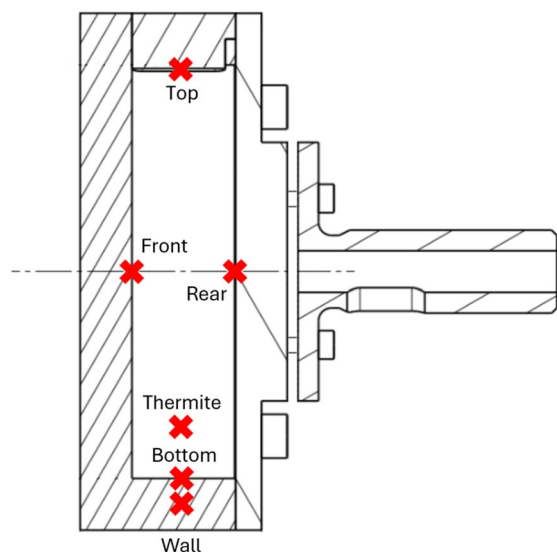
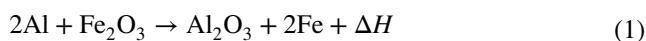


Fig. 2 Position of the thermocouples in the samples

the test. The other instruments that were used to monitor the temperature of the samples are described in Sect. 2.3, being not mounted directly on them.

2.2 Thermite charge

The thermite selected for the tests in the hypersonic wind tunnel was a mixture of aluminum and hematite (iron oxide). This thermite is the most widely used in terrestrial applications, being inexpensive and energetically dense. Moreover, this formulation does not involve any toxic reactant or product, and requires a relatively intense energetic stimulus to be initiated. Considering its one-step theoretical reaction, the oxidation of the starting metal and the reduction of the starting oxide can be described as per Eq. 1.



As reported by Fischer and Grubelich [19], its adiabatic flame temperature is 3135 K, its theoretical heat release ΔH is 3958.20 kJ/kg, and under standard conditions 7.84% of its products (in mass) gasify. The characteristics of the starting powders are reported in Table 1.

As reported in Ref. [18], the ignition temperature in a low oxygen environment of this thermite is around 1500 K.

Table 1 Characteristics of the starting powders

Powder	Characteristics	Purity	Supplier	Batch
Al	Spherical, 30 μm	$\geq 99\%$	AMG Alpoco	N.A
Fe_2O_3	– 325 mesh ($\leq 44 \mu\text{m}$)	98%	Thermo Scientific	M22H036

For the tests presented in this paper, the objective was not to provoke the partial demise of the samples, but only to measure their temperature increase after the thermite ignition. For this reason, a fraction of the thermite was mechanically activated through high-energy ball milling to lower its ignition temperature. Other strategies, such as the use of a finer powder, chemical activation (e.g., [20]), or the use of additives [21] can be used to lower the ignition temperature of the mixture. For this experimental campaign, mechanical activation was preferred to preserve the intrinsic safety of micron-sized powders, and to limit the number of chemical species in the mixture, which could introduce new unknowns from a chemical viewpoint. The activated thermite was then hand-mixed with the standard formulation so that the activated fraction constituted 16% of the total mass. During preliminary hot wire tests at Politecnico di Milano, this mixture showed reliable ignition temperature in the range 1100–1250 K, well before the melting temperature range of steel. This formulation was then selected for the tests on the SADM mock-ups. Table 2 reports the tests that will be presented in this paper, detailing the filling level and the mass of thermite used. The first test was performed without any thermite charge, to provide the reference behavior of the mock-up in the wind tunnel. Then, other three tests were conducted, respectively with a filling level of 14%, 25%, and 33% of the available internal volume (157.08 cm^3). Due to budget limits, it was not possible to conduct additional tests to verify their repeatability. However, similar results for other sample geometries have already been presented in Ref. [18].

2.3 Wind tunnel

The tests were performed in DLR's Cologne L2K arc-heated hypersonic wind tunnel. The facility uses a Huels-type arc heater with a maximum electrical power of 1.4 MW and can reach cold wall heat fluxes of up to 3.0 MW/m^2 at stagnation pressures up to 250 hPa. It is therefore suitable for studying the late phase of the atmospheric re-entry, when the thermite charge is expected to ignite passively thanks to the aerothermal heat load. Hypersonic free stream velocities are reached using a convergent-divergent nozzle. A large operational

Table 2 Filling level and thermite mass of the tests performed with the SADM mock-ups

Test ID	Filling level (%)	Themite mass (g)
1	–	–
2	14	2.7 A + 14.3 T
3	25	4.8 A + 25.1 T
4	33	6.3 A + 33.2 T

The filling level refers to the internal cavity volume (157.08 cm^3). The activated and standard fractions of the charge are respectively marked as “A” and “T”

envelop is ensured by the possibility of changing the nozzle throat and exit diameters. In the tests discussed in this paper, the working gas was air, but it is possible to vary the test gas to create conditions as similar as possible to the ones expected on other planets. An extensive presentation of the characteristics of the L2K wind tunnel can be found in Ref. [22]. For the tests on the SADM mock-ups, a 29 mm wide nozzle throat and a nozzle exit diameter of 200 mm were used. The samples were placed at 120 mm from the nozzle exit. The tunnel was operated at a total pressure of 1400 hPa, a total temperature of 4297 K, and a mass flow rate of 50 g/s, resulting in a cold wall heat flux of 590 kW/m².

Several instruments were used to monitor the temperature evolution of the samples. The optical instrumentation in L2K is shown in Fig. 3. In particular, two pyrometers (Maurer KTRD 1485 and QKTRD 1483) registered the temperature of the center of the front face. Two IR thermocameras (Optris PI 1 M and Infratec VarioCAM HD) acquired further thermal data. Finally, videos of the tests were recorded from different points of view.

2.4 Numerical model

The SCARAB 3.1L software was used to support the design of the SADM mock-up, to select the wind tunnel operating conditions, and to rebuild the tests results. The software was extended with a dedicated model to represent the effects of an exothermic reaction occurring inside the geometry. Generally, SCARAB is used to simulate the complete re-entry of a space object, computing its dynamics, aerodynamics, aerothermodynamics, and fragmentation. Spacecraft components are introduced as simple shapes, named primitives, that can be combined together to create arbitrarily complex geometries. 3D heat conduction between the different primitives and within each primitive is simulated as well. Radiation to

the environment is considered, but radiative heat exchange between the various primitives that form the geometry is not included. Additional information on the models used in SCARAB can be found in Refs. [23, 24].

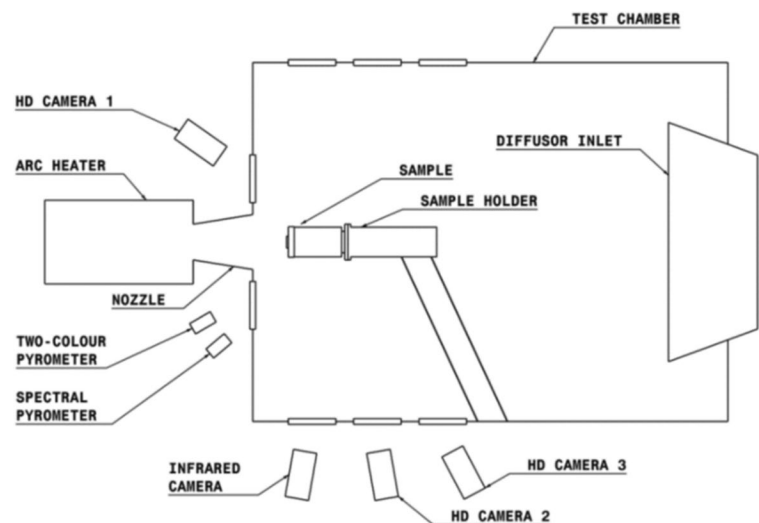
In this case, SCARAB was used in its wind tunnel mode (WTM), a special model framework that excludes object dynamics from the analysis. This approach assumes a constant attitude throughout the simulation, effectively replicating the conditions of wind tunnel tests. Table 3 lists the input parameters for the SCARAB simulations. These values were chosen starting from the operating conditions of the wind tunnel but were later adjusted to match the experimentally measured cold-wall heat flux. The sample holder was not included in the simulations, and consequently, the associated heat flux was neglected.

The thermite charge was introduced as an internal heat source, activated once its ignition temperature is reached by one of the panels that define the thermite cavity. The ignition temperature used in the simulations was the one measured during the experiments. Since the thermite was represented in the model as an internal heat source and not as an additional primitive, it was not possible to assign a mass and specific heat to it. For this reason, the mass and the specific heat of the mock-ups were modified to account for the thermite presence. The starting material properties of the mock-ups were derived from ESA's ESTIMATE database [25]. The

Table 3 SCARAB simulation input parameters

Parameter	Value
Flow velocity	2720 m/s
Density	1.65e−3 kg/m ³
Temperature	652 K
Specific heat ratio	1.42

Fig. 3 Schematic representation of L2K instrumentation



apparent density of the thermite (1190 kg/m^3) was obtained by measuring the weight of a known volume of powder and was considered constant throughout the duration of the experiment. The specific heat of the involved species (both reactants and products) was taken from the NIST-JANAF database [26]. The reaction was considered one-step, happening at the ignition temperature selected by the user. For this reason, at temperatures lower than the ignition one the overall thermite-specific heat was computed starting from the ones of the reactants, while at higher temperatures the ones of the products were used. When the ignition temperature is reached, additional enthalpy is released on the internal panels of the geometry. The overall additional enthalpy budget, ΔH_{add} , is defined as the product of the theoretical enthalpy of reaction, ΔH , multiplied by a coefficient named heat transfer efficiency, η , according to Eq. 2.

$$\Delta H_{\text{add}} = \eta \Delta H \quad (2)$$

This coefficient is used to account for losses that characterize the system, such as incomplete combustion or the ejection of energetic material and energy from the venting holes. Unless otherwise stated for specific test cases, this parameter was considered equal to 60%. This value was determined in a series of preliminary tests in lab-scale conditions at Politecnico di Milano. Once activated, the additional enthalpy is released in a time interval and according to a profile that can be selected by the user. Additional information on the tests conducted to determine the heat transfer efficiency value and the calculation of the heat release profiles can be found in Ref. [27].

The consistency of these hypotheses was verified by comparing the experimental temperature profiles against the temperature evolution of the closest panel of the simulated geometry. Table 4 delineates the correspondence between the experimental and numerical thermocouples, along with the labels used in subsequent sections for reference. Generally, SCARAB primitives are modeled as one-element thick.

Table 4 Correspondence between experimental and numerical thermocouples

Real thermocouple	Numerical thermocouple position	Numerical thermocouple label
Front	Front face, external side	Front_E_WTM
Front	Front face, internal side	Front_I_WTM
Top	Top	Top_WTM
Bottom	Bottom	Bottom_WTM
Inside bottom wall	Bottom	Bottom_WTM
Rear	Rear	Rear_WTM
Thermite	–	–

Refer to Fig. 2 for the nomenclature regarding real thermocouples

Consequently, both the "bottom" and "wall" thermocouples (refer to Fig. 2) were compared against the temperature of the corresponding panel. Instead, a different approach was used for the front face of the sample, which was represented as a layered structure of four metal disks to capture the potentially significant thermal gradient. This distinction arises from the fact that the temperature of the front face is the main driver for the ignition of the internal charge, being the region most rapidly heated by the incoming flow. A pronounced thermal gradient across the front face could significantly influence the timing of thermite ignition. Finally, a last remark should be considered for the thermocouple embedded in the thermite charge during the tests. In this case, it was not possible to select an appropriate panel for the comparison, as the pyrotechnic charge is represented as an internal heat source rather than an independent primitive.

3 Results and discussion

3.1 Reference test without thermite

The experimental campaign started with a reference test involving a SADM mock-up without any internal charge. The main objectives of this test were to characterize the baseline behavior of the sample under the selected test conditions and to highlight potential limits in its representation through the SCARAB 3.1L software.

Figure 4 shows the experimental and numerical results obtained for the front face of the mock-up in the reference test, respectively in solid and dashed lines. The trend of the temperature profile measured by the thermocouple on the front face is in good agreement with the simulation until temperature values around 1200 K. After this moment, the thermocouple signal becomes more noisy and stops its rise. This can be attributed to a partial detachment of the sensor from the wall. However, for higher temperatures, the numerical traces approach the profiles measured by the pyrometers, confirming the ability of SCARAB to capture the physics of the surface directly exposed to the incoming flow. As for the temperature gradient across the front face, the SCARAB simulation suggests a limited but not negligible difference of around 30 K, almost constant over the test duration. This value seems reasonable with respect to the temperature traces measured by the thermocouple and the pyrometers.

The temperature profiles of the upper and lower walls, both experimental and numerical, are reported in Fig. 5. There is no significant difference between the temperature measured on the internal side of the lower wall and that measured inside it. This indicates that the thermocouple inside the wall is a good indicator of the temperature of that portion of the sample. On the contrary, a certain difference can be noticed between the upper and the lower part of the

sample. This could be due to the presence of the lid, which implies a certain thermal resistance. As for the numerical results, the simulated heating rate and maximum temperature are lower than those of the experimental data. However, the steady state is reached in a similar time interval. This behavior is probably due to the heat transfer model used in SCARAB 3.1L, which comprises 3D heat conduction but does not consider radiative heat exchange between the

elements of the model. In addition, vortices and recirculation effects are also not considered. A similar result can be seen in Fig. 6 for the temperature of the rear wall. In this case, a delay of the numerical temperature profile is evident as well. The heat applied on the front face needs some time to propagate through the sample without the contribution of internal radiation, and this is probably the cause of the delay.

Fig. 4 Comparison between experimental (solid lines) and numerical (dashed lines) temperature profiles of the front face for the reference test without thermite (Test 1)

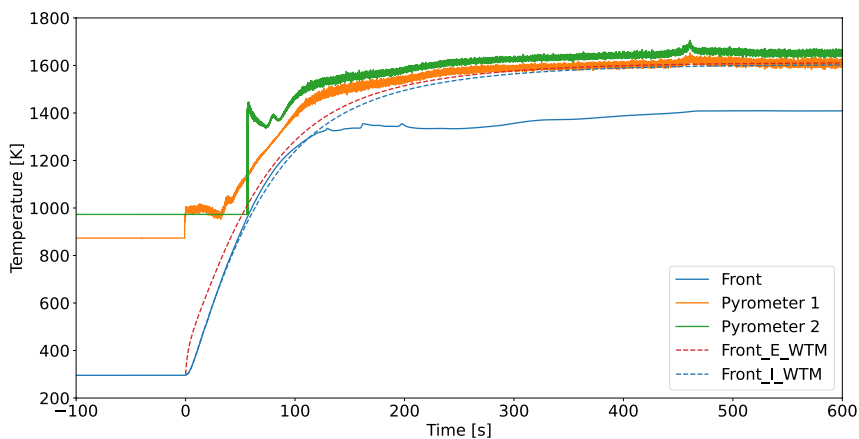


Fig. 5 Comparison between experimental (solid lines) and numerical (dashed lines) temperature profiles of the top and bottom walls for the reference test without thermite (Test 1)

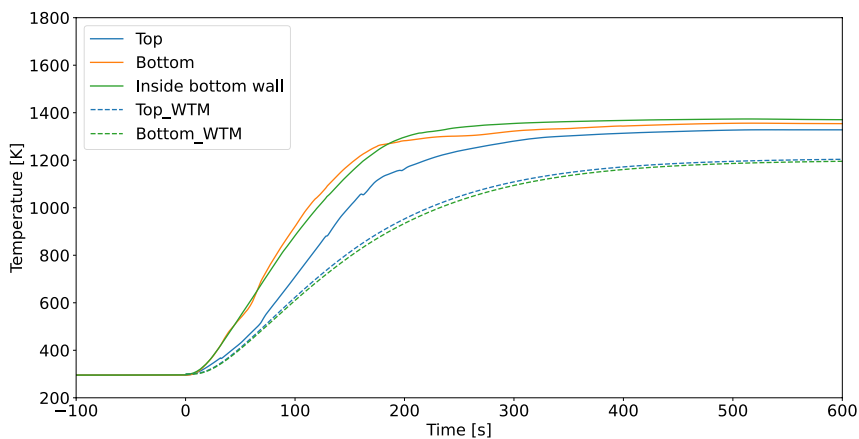
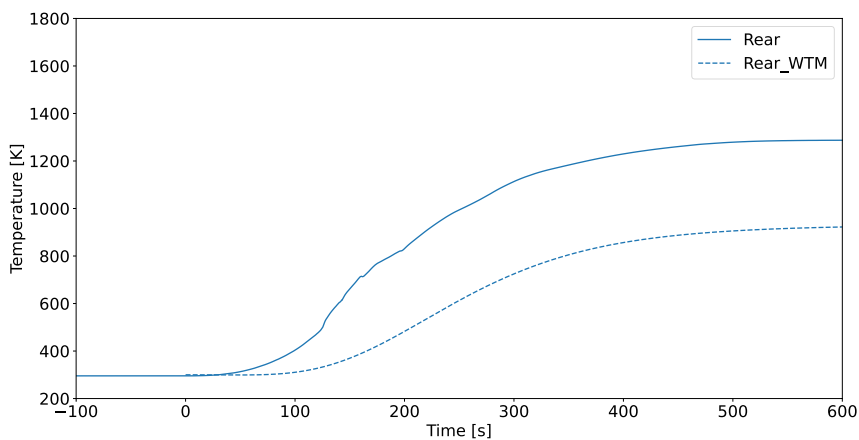


Fig. 6 Comparison between experimental (solid lines) and numerical (dashed lines) temperature profiles of the rear face for the reference test without thermite (Test 1)



3.2 Experimental results of tests involving thermite

As indicated in Table 2, three tests at three different filling levels (14%, 25% and 33%) have been performed to analyze the heat transfer process occurring between the reacting charge and the mock-up. Higher filling values have been avoided due to concerns of possible pressure build-ups which could result in loss of the safety lid and venting out of a significant portion of the energetic material (as reported in Ref. [18]). The comparison between experimental and numerical thermal traces of the tests is available in Appendix 1. In this section, only the key results will be discussed

in detail. Three frames per each test are shown in Fig. 7: the instant of ignition, 5 s after ignition, and 10 s after ignition. All videos share the same camera parameters. The same images, in this case recorded by the IR camera, are shown in Fig. 8. Qualitatively, the intensity of the stream of high-temperature reaction products ejected from the venting holes, just after ignition, seems to increase with the filling level. Similarly, the lower part of the front face of the sample appears brighter after the ignition of a greater quantity of thermite. This result is quantified by the temperature traces measured by the thermocouple inside the wall, reported in Fig. 9. The recorded temperature traces confirm that the

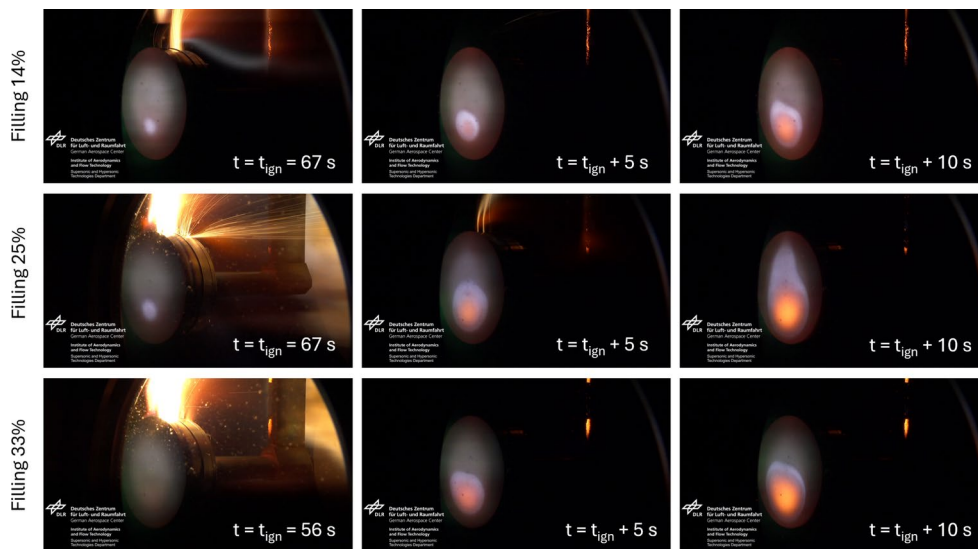
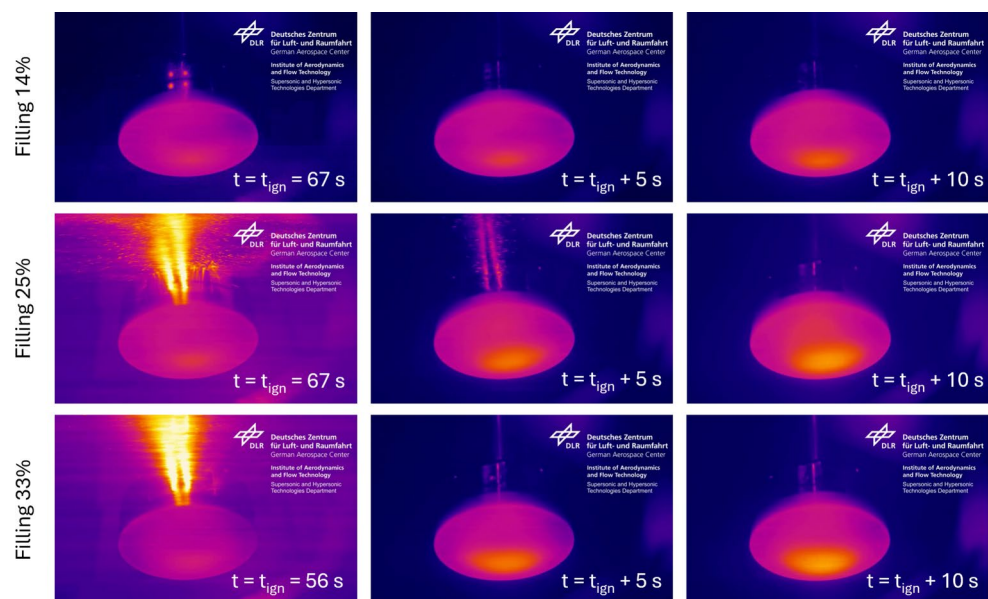


Fig. 7 Recorded images of the tests involving thermite. For each test, the frame of the thermite ignition is reported, as well as the appearance of the sample after 5 and 10 s

Fig. 8 Recorded infrared images of the tests involving thermite. For each test, the frame of the thermite ignition is reported, as well as the appearance of the sample after 5 and 10 s



internal thermite charge was able to transfer additional heat to the mock-up, proving the T4D concept. The heat transfer to the lower part of the sample increases with a higher thermite filling, showing a strong non-linearity when the filling level is changed from 25 to 33%. Moreover, the higher the thermite quantity, the sooner the sustained ignition of the charge. In the test involving the 14% filling, a feeble ignition (67 s) anticipated the sustained one of the rest of the charge (72 s), which occurred well after one of the test involving a filling level of 25% (67 s). In the test with the highest filling level, the ignition occurred after only 56 s. This behavior can be explained as the thermite is a porous medium with limited heat conductivity. In all tests, the same formulation was used (16% of activated thermite dispersed in 84% of standard Al/Fe₂O₃ mixture). The onset of the reactions inside the pyrotechnic charge is expected to happen at repeatable temperature and is driven by the temperature of the front face, which is the portion of the sample that heats up first. A higher filling level implies an obstacle to heat transfer, since a porous pyrotechnic material is a bad thermal conductor; thus, the incoming heat from the front face is not efficiently distributed in the thermite. For these reasons, the temperature of ignition is reached faster in the tests with more thermite. The ignition temperature and time are reported in Table 5. However, sustained ignition for the test at 14% filling occurs only after 72 s; in this case, it is not possible to quantify the sustained ignition temperature as the front thermocouple fails after the first feeble ignition. In Table 5 the charge mass loss is also reported. This quantity is the fraction of thermite that has been ejected through the venting holes during the tests and was computed as per Eq. 3.

$$m_{l\%} = \frac{m_f - m_s}{m_i - m_s}, \quad (3)$$

where $m_{l\%}$ is the charge mass loss, m_s is the mass of the mock-up (including thermocouples), and m_i and m_f are

Fig. 9 Comparison of the temperature profiles measured by the thermocouple embedded in the bottom wall of the samples at various thermite fillings. The markers (stars) indicate the ignition of the powder

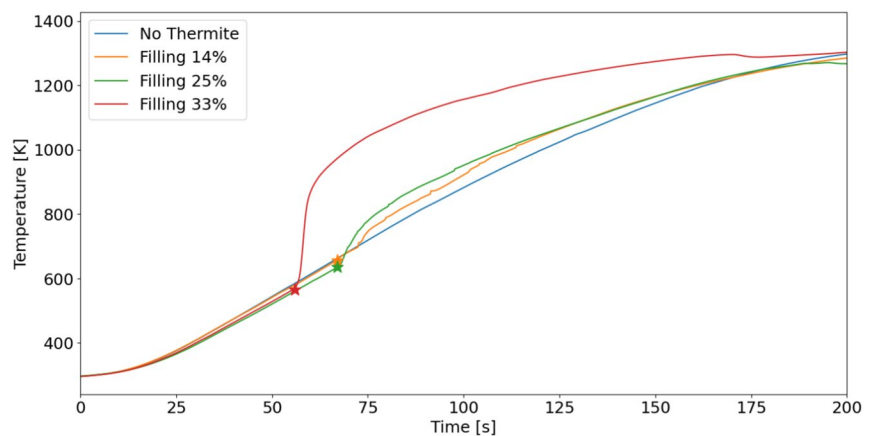


Table 5 Experimental ignition temperature, ignition time, and charge mass loss obtained for the three tests at different filling levels

Test ID	Filling level (%)	Ignition temperature (K)	Ignition time (s)	Charge mass loss, $m_{l\%}$
2	14	1038	67 (72*)	20.0%
3	25	1062	67	11.7%
4	33	948	56	5.3%

*: for Test 2, instant of time for experimental sustained ignition

respectively the initial and final mass of the sample containing thermite, just before and after the test. Even if the thermite charge loss is lower for higher filling levels, a probable increase in the additional available enthalpy for Test 3 and Test 4 would not justify the strong nonlinearity observed between them. A more consistent explanation was obtained when the mock-ups were opened after the tests were completed. In general, the slag that could be found on the internal cavity of the samples was porous and fragile, easily removable with the slight pressure of a spoon or at bare hands. In contrast, in the mockup of Test 4 (filling level 33%) a solidified drop of reaction products was found on the lower part of the internal cavity (Fig. 10a). Then, a radiography was performed to obtain more information on its internal structure and the result can be seen in Fig. 10b. In the conditions used during the radiography, Al₂O₃ is almost transparent, while Fe-based species typically appear as a dark matter. For this reason, the drop appears to be formed by a solid core of iron surrounded by a porous slag of aluminum oxide. The most interesting feature of this structure is the segregation between the product species, which was not evident in any other part of the samples. The creation of this resolidified drop is evidently a result of the conditions of the tests, in which the mock-ups were maintained at constant attitude. This gravitational effect is not expected for a real T4D application, in which the tumbling motion typical

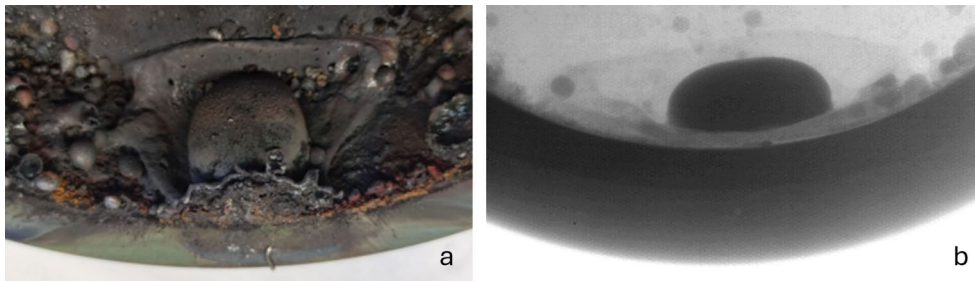


Fig. 10 Drop of solidified products found in the lower part of the mock-up tested with thermite at 33% filling (Test 4). **a** External appearance. **b** Radiography

of re-entering spacecraft should limit these gravitational effects.

3.3 Numerical rebuilding of tests involving thermite

As described in Sect. 2.4, the standard parameters of the thermite heat release model were obtained through a series of tests in lab-scale environment performed at Politecnico di Milano [27]. However, the unexpectedly high temperature increase registered by the thermocouple embedded in the lower wall for Test 4 led to change simulation parameters. For this reason, the numerical rebuilding of Tests 2 and 3 is presented in Sect. 3.3.1, while the one of Test 4 in Sect. 3.3.2.

The adjustment of parameters in the heat release model for Test 4 did not influence the simulations prior to thermite ignition. Consequently, the ability of the SCARAB model to accurately describe the process that leads to ignition remains unaffected by these adjustments. The main parameter of merit for evaluating the model's accuracy in predicting thermite ignition is the difference between the simulated and the experimental ignition times, as the ignition temperature of the charge was derived directly from the front-face thermocouple measurement. Although the front thermocouple was chosen as the reference, all other thermocouples consistently registered ignition at the same instant, in all three tests involving thermite. Table 6 summarizes the results concerning the ignition time. As the geometry and heat load are the same for all simulations, the numerical ignition time is a direct function of the ignition temperature, which is detailed in Table 5. In all three cases, the numerical model is able to predict the thermite ignition with an error margin of less than 5 s. This result is in good agreement with the ones obtained for the tests on the ball-bearing unit mock-ups discussed in Ref. [18]. Similarly, in that case, SCARAB was able to describe with good accuracy the ignition of the thermite at relatively low filling levels (< 50%), while for higher fillings a consistent delay of numerical ignition was registered, especially if the thermite was characterized by a

Table 6 Comparison between experimental and numerical ignition time

Test ID	Filling level (%)	Experimental ignition time (s)	Numerical ignition time (s)	Difference (s)
2	14	67 (72*)	68	1
3	25	67	72	5
4	33	56	59	3

For Test 2, experimental sustained ignition is indicated with an asterisk

rather high ignition temperature. This is probably due to the insulating effect of the thermite, which is not properly represented in the numerical model and which becomes more evident at high temperature.

3.3.1 Tests at 14% and 25% filling levels

The rebuilding of the tests involving filling levels of 14% and 25% were carried out with standard parameters for the thermite heat release already used in Ref. [18]. The heat transfer efficiency η was set to 60%, and the heat was released uniformly across a time frame of 10 s (step-like profile).

The temperature increments caused by the thermite ignition on the front face and on the lower wall are reported in Figs. 11 and 12, for both the experimental and numerical tests involving the 14% filling level. As it can be seen in Fig. 12, during this test multiple ignitions of the thermite charge were experienced. As already observed in Sect. 3.1, the lower wall temperature is underestimated by the software. Nevertheless, it is possible to evaluate the adequateness of the thermite model by considering the temperature increments upon reaction that are measured during the experiment and computed by the software. In Fig. 11 the temperature increments that can be seen in the experimental and numerical data are highlighted, as well as the duration of the thermite heat release in the SCARAB model. The temperature trend seems reasonably captured both in terms of duration and temperature increase. In particular,

the experimental and numerical temperature increments are reported in Table 7. The simulation overestimates the temperature increase of the front face and underestimates the one of the lower wall, but the general heat transfer seems adequately predicted.

Similarly, the experimental and numerical results for the test at 25% filling level are reported in Figs. 13 and 14. In this test, the thermite charge reacted more regularly. Also

in this case the temperature trend obtained by simulation appears qualitatively to be in good agreement with the experimental data, confirming that 60% is a reasonable value for the heat transfer efficiency η . The comparison between the experimental and simulated temperature increase in Table 7 shows that, for this test, the thermite effect on the front face is slightly underestimated. The difference increases for the lower wall. This could be due to the internal dynamics of the

Fig. 11 Temperature increase on the front face of the mock-up upon thermite reaction for the 14% filling level (Test 2). Experimental temperature traces are in solid lines, while numerical results in dashed lines. The markers indicate the experimental (star) and numerical (circle) ignition

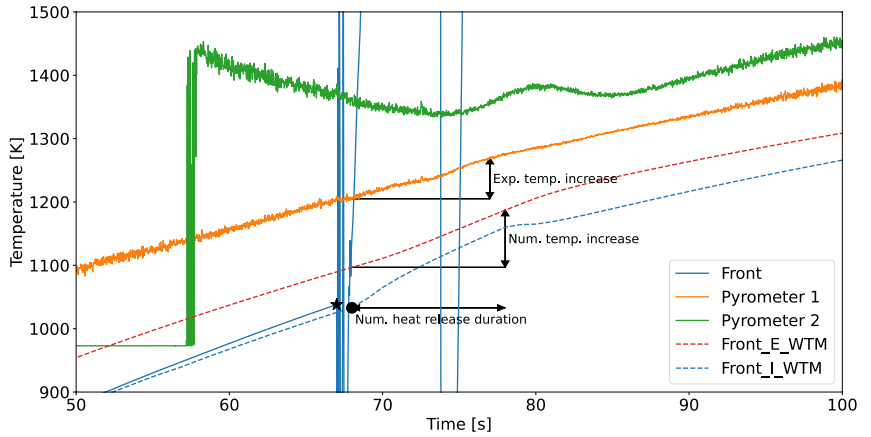


Fig. 12 Temperature increase on the top and bottom walls of the mock-up upon thermite reaction for the 14% filling level (Test 2). Experimental temperature traces are in solid lines, while numerical results in dashed lines

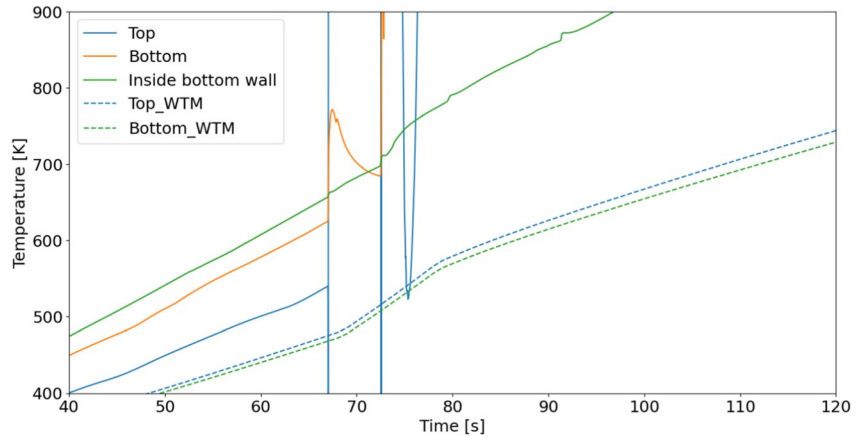


Fig. 13 Temperature increase on the front face of the mock-up upon thermite reaction for the 25% filling level (Test 3). Experimental temperature traces are in solid lines, while numerical results in dashed lines

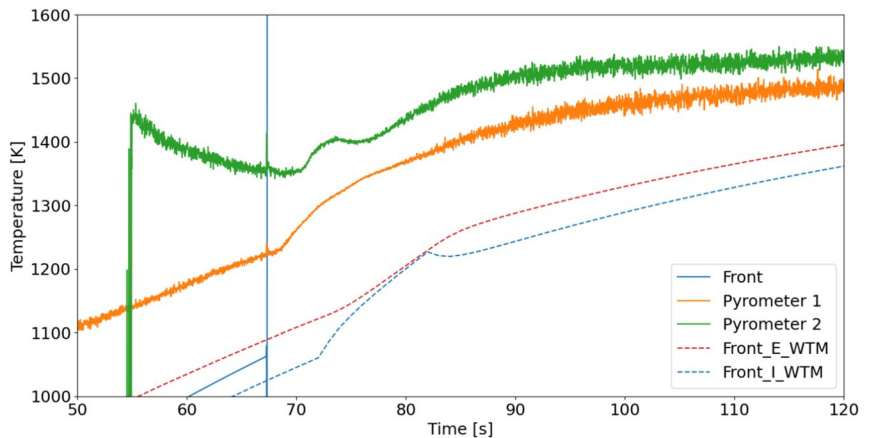


Fig. 14 Temperature increase on the top and bottom walls of the mock-up upon thermite reaction for the 25% filling level (Test 3). Experimental temperature traces are in solid lines, while numerical results in dashed lines

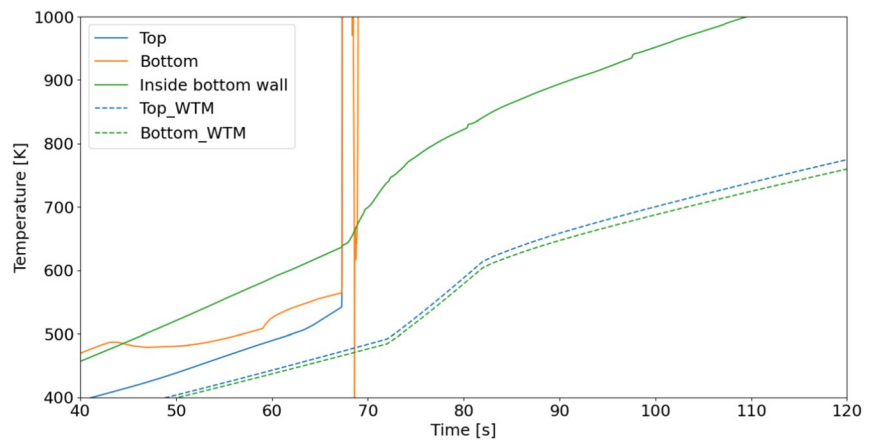


Table 7 Comparison between experimental and numerical temperature increase of front and lower walls for Tests 2 and 3, considering a time interval of 10 s after the thermite ignition

Test ID	Surface	Exp. temperature increase (K)	Num. temperature increase (K)	Difference (%)
2	Front	70	91	30
2	Lower	109	93	- 15
3	Front	126	114	- 10
3	Lower	163	121	- 26

The front face and the lower wall temperature increments were respectively computed considering the data measured by the Pyrometer 1 and the thermocouple embedded in the lower wall

molten products, gradually reaching the condition observed for Test 4. However, the resolidified products within the cavity of the mock-up tested at 25% filling level were homogeneously distributed and there was no sign of agglomeration.

3.3.2 Test at 33% filling level

The consistent temperature increase caused by the thermite on the mock-up tested at 33% filling level led to a different simulation approach. In fact, the standard set of parameters led to a significantly lower temperature increase than the one registered by the thermocouple embedded in the lower wall. For this reason, the heat transfer efficiency η was increased to unity and the additional heat provided by thermite was applied only on the lower half of the front face and of the lateral wall.

The comparison between the experimental data and simulation results is shown in Figs. 15 and 16. As it can be seen in Fig. 15, with these settings the numerical temperature increase of the front face (external side) is significantly higher than the one measured experimentally (Pyrometers 1 and 2). However, the simulated temperature of the lower wall is still lower than the experimental data (Fig. 16). As it is shown in Table 8, the simulated temperature increase within 10 s after thermite ignition is higher than that recorded in the experiment, but the experimental mock-up receives heat for a longer time. This is caused by the residence of high-temperature products in proximity to

Fig. 15 Temperature increase on the front face of the mock-up upon thermite reaction for the 33% filling level (Test 4). Experimental temperature traces are in solid lines, while numerical results in dashed lines

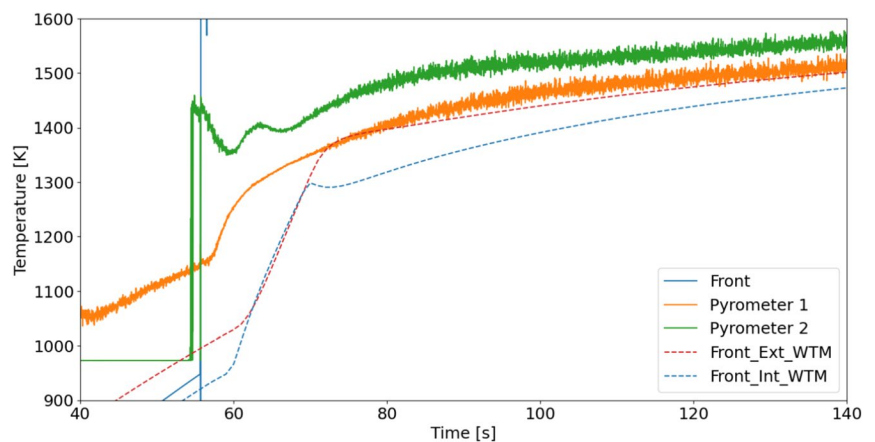


Fig. 16 Temperature increase on the top and bottom walls of the mock-up upon thermite reaction for the 33% filling level (Test 4). Experimental temperature traces are in solid lines, while numerical results in dashed lines

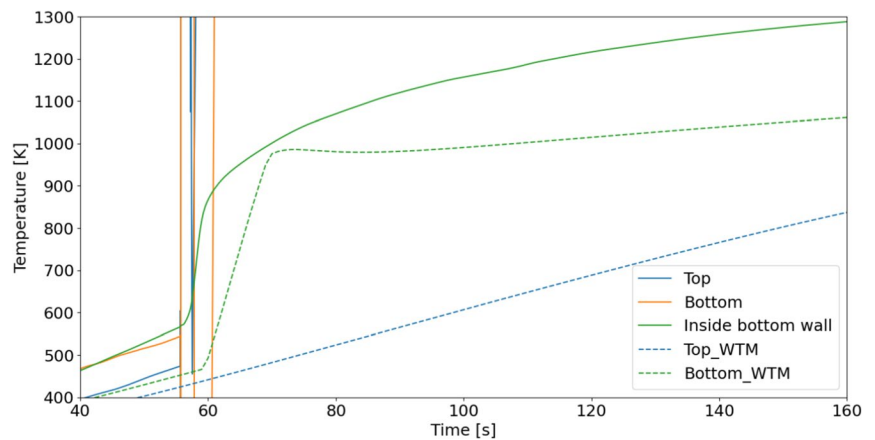


Table 8 Comparison between experimental and numerical temperature increase of front and lower walls for Test 4, considering a time interval of 10 s after the thermite ignition

Test ID	Surface	Exp. temperature increase (K)	Num. temperature increase (K)	Difference (%)
4	Front	169	295	75
4	Lower	392	485	24

The front face and the lower wall temperature increments were respectively computed considering the data measured by the Pyrometer 1 and the thermocouple embedded in the lower wall

the thermocouple lodged inside the wall. This process is not well captured by the numerical model.

4 Conclusion

In this paper, the results of the experiments performed in the frame of the ESA-TRP SPADEXO project on SADM-inspired geometries were presented. The objective of these tests was to study how the heat generated from a reacting thermite, placed internally to the target, was transferred to the surrounding structure depending on the filling level. The steel mock-ups were designed with a slot to accommodate a thermocouple, ensuring its reliability throughout the duration of the tests. The samples have been filled with Al/Fe₂O₃ thermite and exposed to the high-enthalpy hypersonic flow produced by DLR's L2K wind tunnel.

A reference test without pyrotechnic charge and three tests involving thermite were conducted. The thermite ignited reliably in all tests, causing a measurable temperature

increase in the vessels. The thermite effect measured by the thermocouple embedded in the wall increased with higher filling, showing a nonlinear behavior. The main reason was the deposition of a drop of high-temperature reaction products that transferred heat through conduction to the surrounding part of the mock-up. A radiography performed on the drop revealed that it was formed by a solid material (probably Fe-based species) surrounded by a porous slag, more transparent to X-rays (probably Al-based species). All other samples presented a porous and fragile slag uniformly distributed on the internal surface.

The experimental tests were later rebuilt using ESA's SCARAB 3.1L software, using its wind tunnel mode. The simulation of the reference test without thermite revealed a very good agreement between experimental and numerical results of the front face, while the SCARAB simulation resulted in a lower temperature for the lateral and rear surfaces. This is probably due to the absence of internal radiation and recirculation flows in the numerical model. The SCARAB extension implemented for representing the thermite action was able to appropriately describe the ignition process of the charge, resulting in a few seconds of delay with respect to the numerical results. For tests involving a filling level of 14% and 25%, a heat transfer efficiency of 60% was used. The results indicated that this value is reasonable to represent the overall heat transfer from the reacting thermite to the surrounding structure. In contrast, the test at 33% filling level was not appropriately described with this simulation parameter, as the numerical temperature increase was too low to depict the effect of the drop of reaction products. For this reason, the simulation was run with unity heat transfer efficiency, and the heat was released only on the lower half of the geometry. The final results for this

test showed how the temperature increase of the front face was overestimated by the simulation, while the heat transfer from the drop to the lower wall was more intense, even if slower, with respect to the numerical rebuilding.

These results show how the internal dynamics of the reaction products are paramount in determining the heat transfer to the target. The tendency to create agglomerates seems to increase with the filling level. It can be expected that thermites with lower gas production could enhance this behavior as well. This mechanism could be exploited to direct the reaction enthalpy in strategic points of the space equipment. However, the tumbling motion typical of re-entering spacecraft is expected to limit this effect. In general, these experiments proved that a reacting thermite can transfer a significant fraction of its reaction enthalpy to its enclosing vessel. This strongly encourages further research on the topic. Moreover, the use of formulations capable of reacting without the release of gaseous products could enable the testing of samples at higher filling levels, therefore increasing the

additional enthalpy provided by the exothermic reaction. From a simulation viewpoint, a more detailed model of the thermite reaction, represented in this paper as a simple one-step event, could improve the description of its effect on the component to be demised. In addition, the comparison of the numerical results with similar simulations performed with a different re-entry tool could help in decoupling the effects of the thermite from tool-specific features, such as radiation modeling approach.

Appendix 1: Temperature traces of tests involving thermite

In Figs. 17, 18, 19, 20, 21, 22, 23, 24 and 25, the comparison between the experimental and numerical temperature traces of the tests involving thermite is reported.

Fig. 17 Comparison between experimental (solid lines) and numerical (dashed lines) temperature profiles of the front face for Test 2 (14% filling level)

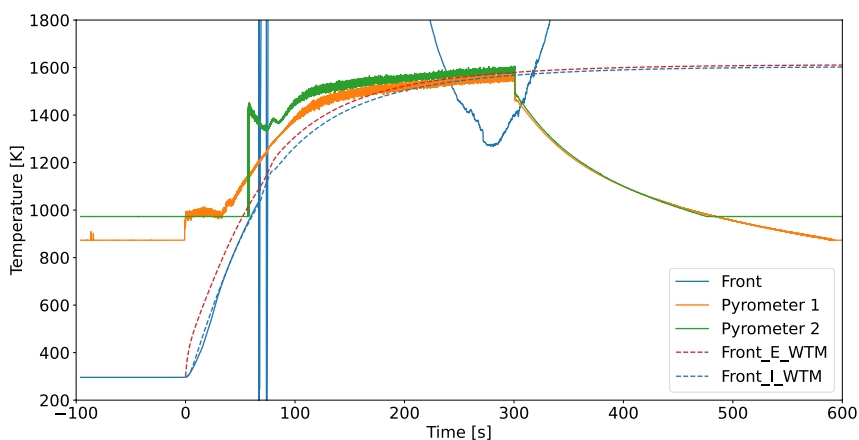


Fig. 18 Comparison between experimental (solid lines) and numerical (dashed lines) temperature profiles of the top and bottom walls for Test 2 (14% filling level)

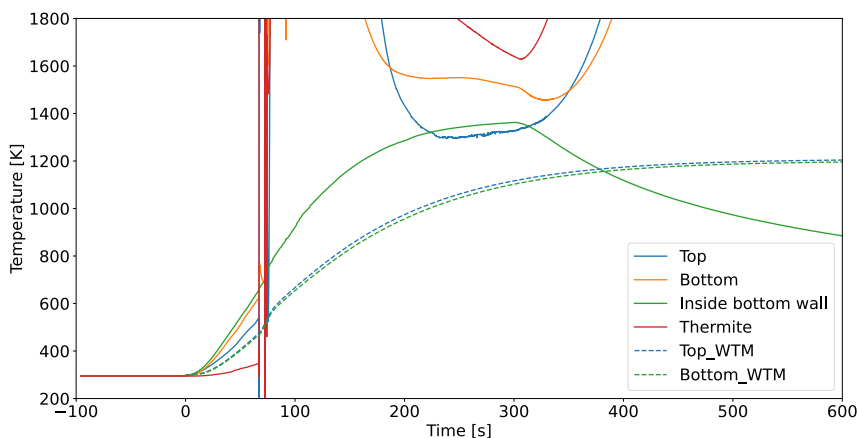


Fig. 19 Comparison between experimental (solid lines) and numerical (dashed lines) temperature profiles of the rear face for Test 2 (14% filling level)

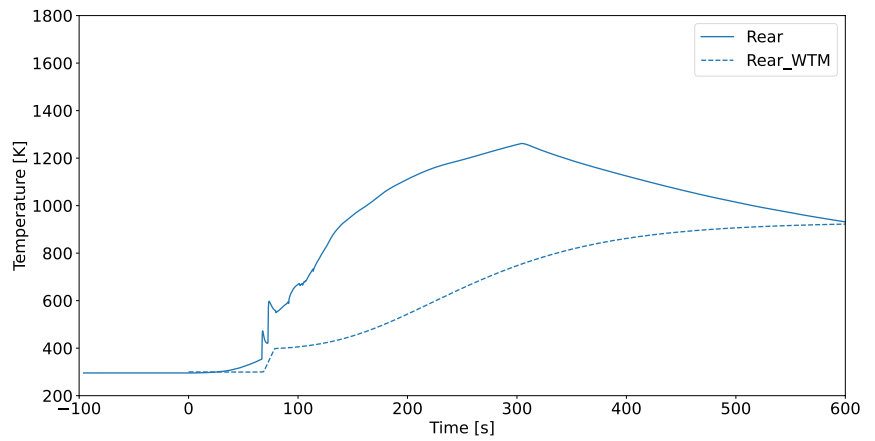


Fig. 20 Comparison between experimental (solid lines) and numerical (dashed lines) temperature profiles of the front face for Test 3 (25% filling level)

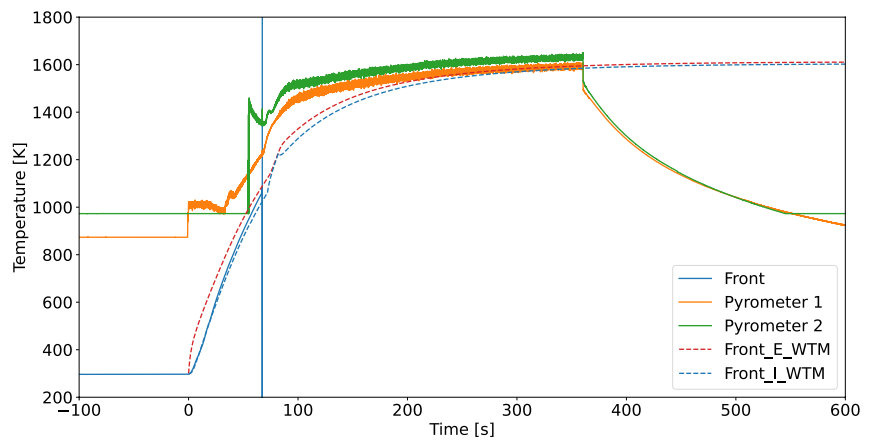


Fig. 21 Comparison between experimental (solid lines) and numerical (dashed lines) temperature profiles of the top and bottom walls for Test 3 (25% filling level)

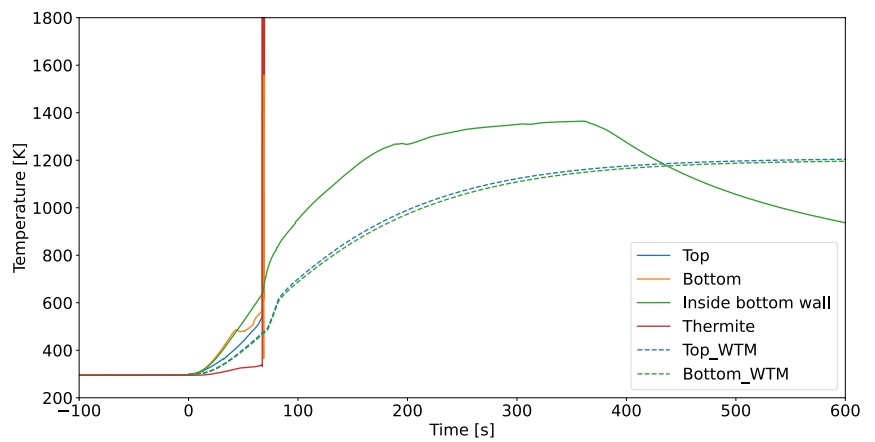


Fig. 22 Comparison between experimental (solid lines) and numerical (dashed lines) temperature profiles of the rear face for Test 3 (25% filling level)

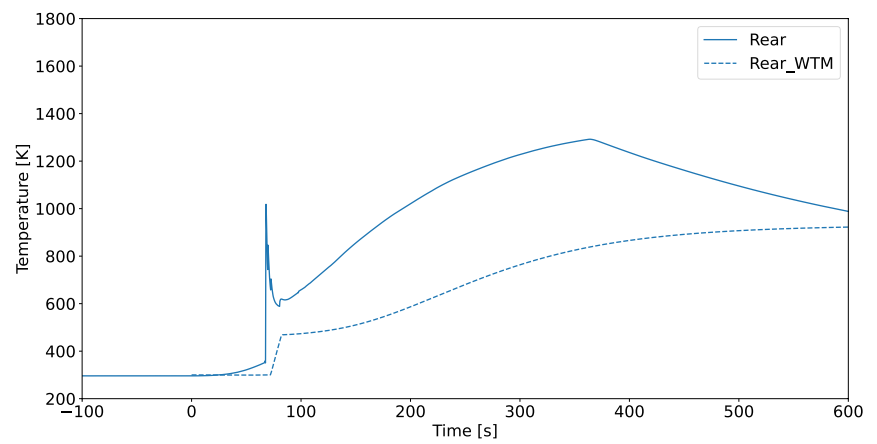


Fig. 23 Comparison between experimental (solid lines) and numerical (dashed lines) temperature profiles of the front face for Test 4 (33% filling level)

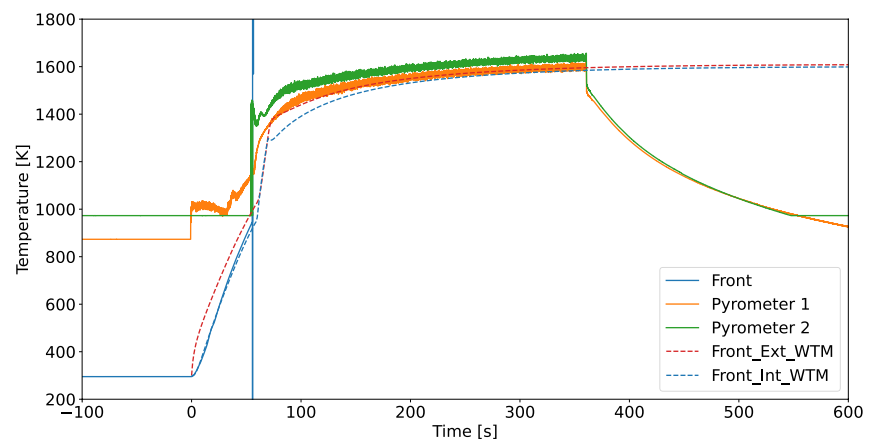


Fig. 24 Comparison between experimental (solid lines) and numerical (dashed lines) temperature profiles of the top and bottom walls for Test 4 (33% filling level)

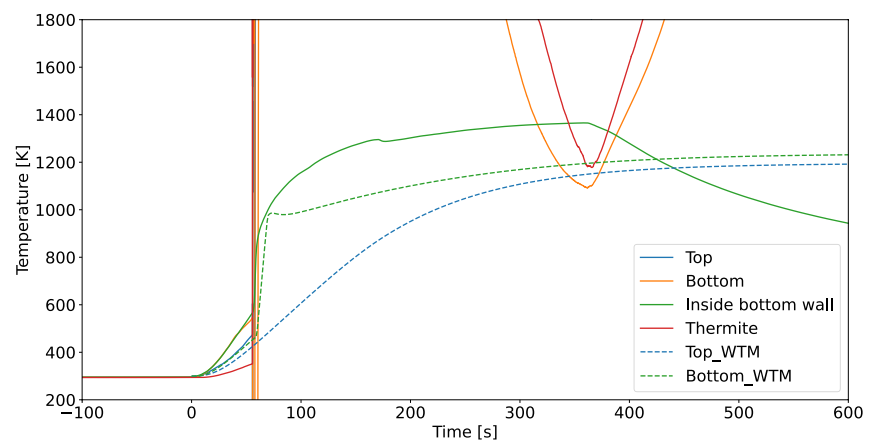
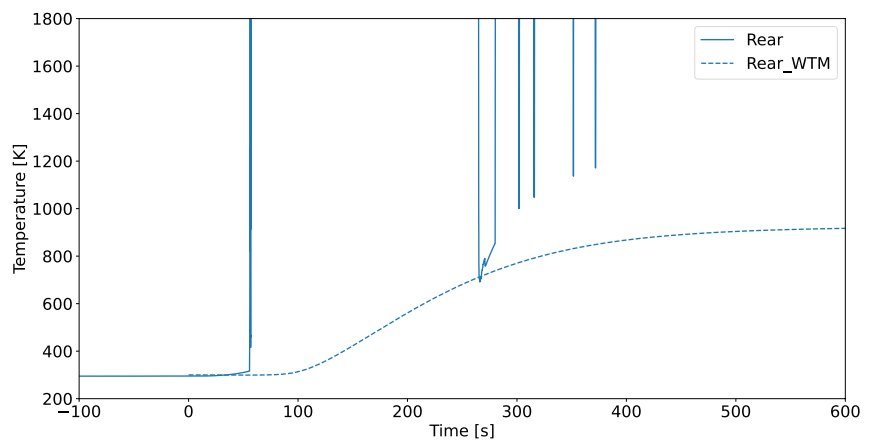


Fig. 25 Comparison between experimental (solid lines) and numerical (dashed lines) temperature profiles of the rear face for Test 4 (33% filling level)



Acknowledgements The research presented in this paper has been performed in the framework of the ESA-TRP SPADEXO project, contract number ESA AO/1-10812/21/NL/MG. The authors gratefully acknowledge the help and advice of the technical staff of the DLR Supersonic and Hypersonic Technologies Department.

Funding Open access funding provided by Politecnico di Milano within the CRUI-CARE Agreement.

Data availability Raw thermocouple data from samples tested in wind tunnels are available upon request. Authorization from the funding entity is required to access this data.

Declarations

Conflict of interest The thermites used in this work have been produced by the company ReActive Powder Technology s.r.l.; Filippo Maggi, Christian Paravan, and Stefano Dossi are co-founders of ReActive Powder Technology s.r.l.

Open Access This article is licensed under a Creative Commons Attribution 4.0 International License, which permits use, sharing, adaptation, distribution and reproduction in any medium or format, as long as you give appropriate credit to the original author(s) and the source, provide a link to the Creative Commons licence, and indicate if changes were made. The images or other third party material in this article are included in the article's Creative Commons licence, unless indicated otherwise in a credit line to the material. If material is not included in the article's Creative Commons licence and your intended use is not permitted by statutory regulation or exceeds the permitted use, you will need to obtain permission directly from the copyright holder. To view a copy of this licence, visit <http://creativecommons.org/licenses/by/4.0/>.

References

1. Anonym: ESA's annual space environment report. Technical report GEN-DB-LOG-00288-OPS-SD, European Space Agency, Darmstadt, Germany (2024)
2. Jones, H.W.: The recent large reduction in space launch cost. In: 48th International Conference on Environmental Systems, Albuquerque, New Mexico, USA (2018)
3. Kessler, D.J., Cour-Palais, B.G.: Collision frequency of artificial satellites: the creation of a debris belt. *J. Geophys. Res.* **83**(A6), 2637–2646 (1978). <https://doi.org/10.1029/JA083iA06p02637>
4. Pardini, C., Anselmo, L.: Evaluating the impact of space activities in low earth orbit. *Acta Astronaut.* **184**, 11–12 (2021). <https://doi.org/10.1016/j.actaastro.2021.03.030>
5. Anonym: IADC space debris mitigation guidelines. Technical report IADC-02-01, Revision 3, Inter-Agency Space Debris Coordination Committee (2021)
6. AA. VV.: ESA space debris mitigation requirements. Technical report ESSB-ST-U-007, European Space Agency. Issue 1, Revision 0 (2023)
7. Anonym: Space innovation; mitigation of orbital debris in the new space age. Technical report FCC-CIRC2209-01, Federal Communications Commission (2022)
8. Cattani, B.M., Caiazzo, A., Lemmens, S., Innocenti, L.: An overview of design for demise technologies. In: 8th European Conference on Space Debris, Darmstadt, Germany (2021)
9. Steenbergen, M.J.M.M., Bezooijen, R.W.: Rail welds. In: Lewis, R., Olofsson, U. (eds.) *Wheel-rail Interface Handbook*, Chap. 12, p. 377408. Woodhead Publishing in Mechanical Engineering, Cambridge, UK (2009)
10. Turner, S.: Thermite cutting device. Patent GB 2312864A (1997)
11. Junghare, S., Kumari, S., Chaudhary, A., Kumar, R., Rayalu, S.: Thermite reaction driven pyrotechnic formulation with promising functional performance and reduced emissions. *J. Hazard. Mater.* (2022). <https://doi.org/10.1016/j.jhazmat.2021.127345>
12. Dihlan, D., Omary, P.: Élement de véhicule spatial a capacité d'autodestruction améliorée et procédure de fabrication d'un tel élément. Patent FR 2975080B1 (2011)
13. Seiler, R., Smet, G.: Exothermic reaction aided spacecraft demise during re-entry. Patent EU 3604143A1 (2018)
14. Monogarov, K.A., Pivkina, A.N., Grishin, L.I., Frolov, Y.V., Dilhan, D.: Uncontrolled re-entry of satellite parts after finishing their mission in leo: titanium alloy degradation by thermite reaction energy. *Acta Astronaut.* **135**, 69–75 (2017). <https://doi.org/10.1016/j.actaastro.2016.10.031>
15. Monogarov, K.A., Melnikov, I.N., Drozdov, S.M., Dilhan, D., Frolov, Y.V., Muravyev, N.V., Pivkina, A.N.: Pyrotechnic approach to space debris destruction: from thermal modeling to hypersonic wind tunnel tests. *Acta Astronaut.* **172**, 47–55 (2020). <https://doi.org/10.1016/j.actaastro.2020.03.028>
16. Schleutker, T., Gülhan, A., Esser, B., Lips, T.: ERASD—exothermic reaction aided spacecraft demise—proof of concept testing. Technical report ERASD_TR, DLR, Supersonic and Hypersonic Technologies Department (2019)
17. Daub, D., Finazzi, A., Maggi, F., Lips, T., Kärräng, P.: SPADEXO test report and numerical rebuilding, test report wp 3210, wp 3310

- (d7). Technical report, DLR, Supersonic and Hypersonic Technologies Department (2023)
18. Finazzi, A., Daub, D., Maggi, F., Paravan, C., Dossi, S., Lips, T., Smet, G., Bodjona, K.: Thermite-for-demise (T4D): experiments and numerical modelling on ball-bearing unit mock-ups containing thermite in an arc-heated wind tunnel. *Acta Astronaut.* **223**, 550–576 (2024). <https://doi.org/10.1016/j.actaastro.2024.06.013>
 19. Fischer, S.H., Grubelich, M.C.: Theoretical energy release of thermites, intermetallics, and combustible metals. In: Proceedings of the 24th International Pyrotechnics Society, California, USA (1998)
 20. Chen, A., Wu, B., Li, X., Shen, J., Tian, L., Zhou, Y., Pei, C.: Pushing the limits of energy performance in micron-sized thermite: core-shell assembled liquid metal-modified al@fe₂o₃ thermites. *ACS Appl. Energy* (2021). <https://doi.org/10.1021/acsaem.1c02549>
 21. Song, E., Tracy, G.V.: Incendiary device. Patent US 6766744B1 (2004)
 22. Gülhan, A., Esser, B.: Arc-heated facilities as a tool to study aerothermodynamic problems of reentry vehicles. In: Lu, F.K., Marren, D.E. (eds.) *Advanced Hypersonic Test Facilities*, pp. 375–403. American Institute of Aeronautics and Astronautics Inc, Reston (2002)
 23. Lips, T., Fritsche, B., Homeister, M., Koppenwallner, G., Klinkrad, H., Toussaint, M.: Re-entry risk assessment for launchers development of the new SCARAB 3.1L. In: Proceedings of the Second IAASS Conference, Chicago, USA (2007)
 24. Kanzler, R., Fritsche, B., Lips, T., Breslau, A., Pagan, A., Herdrich, G., Spel, M., Sanvido, S., Lemmens, S.: SCARAB4—extension of the high-fidelity re-entry break-up simulation software based on new measurement types. In: Proceedings of the 8th European Conference on Space Debris, Darmstadt, Germany (2021)
 25. Anon: European Space maTerIal deMisability dATabasE. <https://estimate.sdo.esoc.esa.int/> (2024). Accessed 24 July 2024
 26. Anon: NIST-JANAF Tables. <https://janaf.nist.gov/> (2024). Accessed 24 July 2024
 27. Finazzi, A., Finocchi, P., Carlotti, S., Maggi, F.: Thermite-for-demise (T4D): experimental analysis of heat transfer principles and preliminary sizing of an application. *Int. J. Heat Mass Transf.* (2024). <https://doi.org/10.1016/j.ijheatmasstransfer.2023.124957>

Publisher's Note Springer Nature remains neutral with regard to jurisdictional claims in published maps and institutional affiliations.